Proceedings of ASME Turbo Expo 2011
GT2011
June 6-10, 2011, Vancouver, British Columbia, Canada

GT2011-46331

EXPERIMENTAL AND NUMERICAL INVESTIGATION OF A COMBUSTOR MODEL

Darioush G Barhaghi
Jacek Janczewski
Thomas Larsson
Siemens Industrial Turbomachinery AB
SE-612 83 Finspong, Sweden

ABSTRACT

Fluid flow behaviour is studied both experimentally and numerically in a combustor model which is recently designed at Siemens Turbomachinery AB at Finspong. The model consists of a full size combustor sector that is surrounded by two half size combustor sectors. The half size sectors provide the pressure drop equal to a full scale combustor sector to guarantee the correct air mass flow distribution through the system.

Measurements are performed at atmospheric condition and therefore the boundary conditions are scaled based on the Mach number. This means that the Mach number in different parts of the combustor under the test condition is equal to the Mach number of the flow at full load condition. Pitot tubes and pressure taps are employed to measure the dynamic and static pressures at different cross sections of the model. From the measured pressure, the velocity is calculated.

The pressure distributions along the diffusers are compared and the pressure recovery factor is calculated for different cases.

The computations are performed using RANS (SST k-ω model) and LES (Smagorinsky sub-grid scale model) methods. The computed and measured results show similar trends although there are rather large discrepancies between the results.

NOMENCLATURE

η	Diffuser overall effectiveness
AR	Diffuser outlet to inlet area Ratio
C_p	Pressure recovery coefficient
CFD	Computational Fluid Dynamics
LES	Large Eddy Simulation
L	Length
L_0	Reference length
P_{dyn}	Dynamic pressure
P_{st}	Static pressure
P_{tot}	Total pressure
RANS	Reynolds Averaged Navier-Stokes equations
SGS	Sub-Grid Scale
SIT	Siemens Industrial Turbomachinery AB at Finspong
URANS	Unsteady RANS
U	Velocity
y^+	Distance from the wall in viscous units

INTRODUCTION

Siemens Industrial Turbomachinery AB at Finspong has developed several gas turbines in the range of 15-50 MW [1]. Recently, a new 37 MW gas turbine which is called SGT-750 [2] is added to this family. This gas turbine has a can (tubular) type combustor which is unique in the gas turbine family of SIT and except for the SGT-500 [3] which has a can-annular type combustor all other gas turbines have an annular type combustor.

The combustor of SGT-750 features a newly designed burner. The burner has a radial swirl generator. The swirling flow creates a recirculation zone that together with the pilot stabilizes the flame. Therefore no sudden expansion is employed after the burner exit.

The procedure in design and study of a combustor includes three general steps. In the first step burner and combustor are usually studied at non-reacting atmospheric conditions. In the second and third steps, the system is studied at atmospheric and high pressure under reacting conditions, respectively. As a first step in this work, a model combustor is made of Perspex and tested at atmospheric non-reacting condition. This will help us to improve the performance of the combustor as well as verifying the CFD tools in the company.

This work is divided into two parts. In the first part, the experimental setup is explained and in the second part, the numerical results are shown and compared to the measurements.

EXPERIMENTAL RIG

The experimental rig comprises a full size can-combustor in the center of the model completed with two half size pseudo-combustors. This is shown in Fig 1.

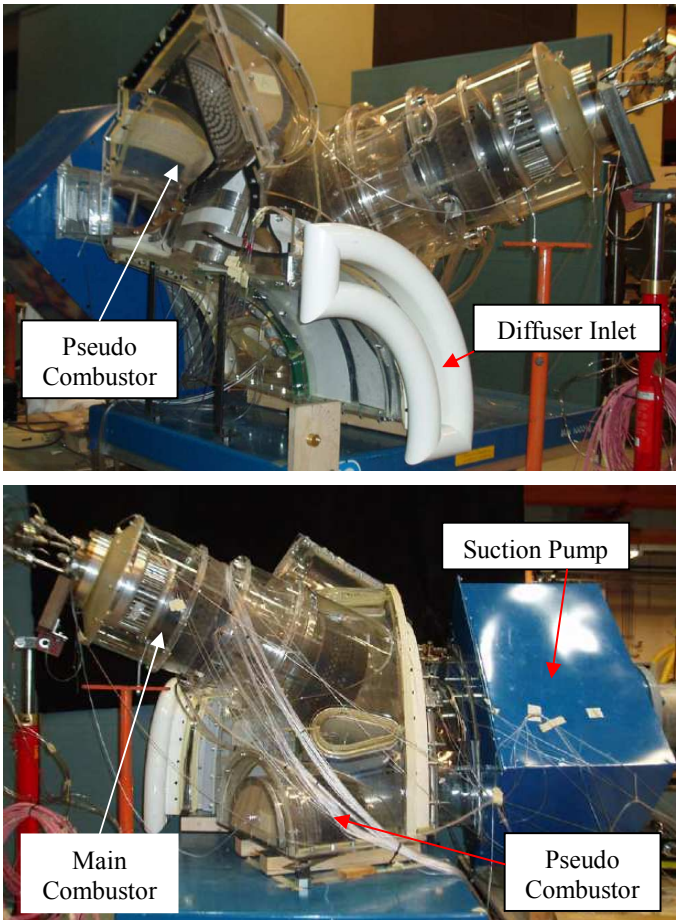

Figure 1: Experimental model of the combustor. The full scale combustor sector is surrounded by two pseudo combustors.

Except for the burner, most of the model is made of a transparent material in order to provide optical access. The components are manufactured by rapid prototyping and casting.

The two half size pseudo-combustors are designed so that the pressure drop in each of them is equal to half of the full scale combustor sector. This will guarantee correct air mass flow through the main combustor sector. The reason why the two pseudo-combustors are included in the model is that this will make the verification of the computations more accurate. Since the CFD model consists of just one sector model with periodic boundary conditions in the span-wise (angular) direction, the experimental model configuration creates such a condition at the plane in the middle of the full and half size sectors.

The air flows through the combustor rig model by sucking the air from the outlet of the combustor. The air mass flow rate is measured by employing a V-cone (McCrometer) which is located between the combustor exit and the pump [4]. The model is instrumented by 128 pieces of pressure taps that are located in the most important spots among which are the diffuser outlet, cooling channel and combustor exit.

The diffuser guides the compressed air to the combustor and is located at the inlet of the combustor. Static pressure taps are placed at the center-line of the diffuser to measure the pressure recovery of the diffuser. In order to have a smooth flow into the domain, curved plates are placed at the inlet edge of the diffusers (look at the white metal at the inlet of the diffuser in Fig 1).

In order to find the recirculation zone in the can, a flow directional probe is traversed along the axis of the can. The change in the sign of the pressure difference that is measured by the probe yields the stagnation point in the flow.

FLOW CONFIGURATION

Fig. 2 shows how the air flows through the combustor model. The air enters the model via diffuser. At the exit of the diffuser, the air splits and some part flows directly into the Tduct via small holes that are located on it. This is shown by the blue lines in Fig. 2. The rest of the air flows through the cooling channel (shown by purple lines) and some part of it enters the swirl generator and the rest ends up in the pilot (the green lines). The swirling flow enters the can and continues towards the exit of the combustor. The highly swirling flow generates a recirculation zone which is shown by orange lines. It should be emphasized that the air flows smoothly into the can and no sudden expansion is employed after the burner.

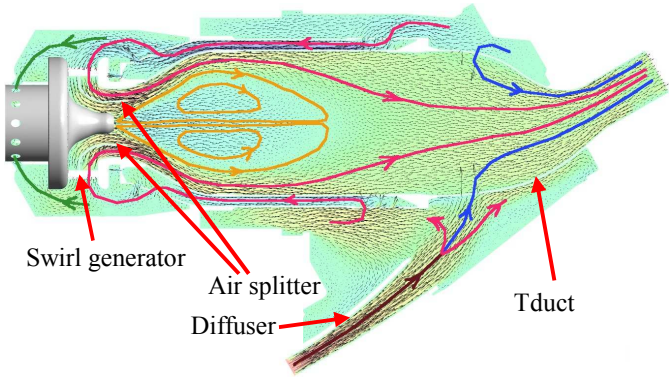

Figure 2: Flow configuration in the combustor model.

CFD MODELLING

Only the main sector of this combustor is modeled by CFD calculations. Since the pseudo-combustor sectors are

eliminated, periodic boundary conditions are applied at the span-wise (angular) direction. In this way it is possible to concentrate more cells in the areas of interest.

Ansys ICEM 12.1 is used to generate the mesh which is mainly composed of unstructured tetrahedral cells. In the cooling channel, three layers of prism cells (pentahedral) are generated near the walls. There are about 22 million cells in the grid. The cell size near the axis of the can is also reduced in order to predict the recirculation zone more accurately. A part of the mesh is shown in Fig 3.

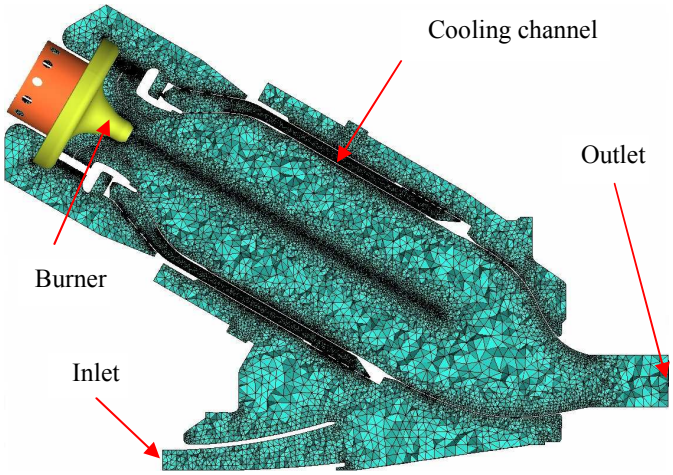

Figure 3: Mesh concentration in the computational domain.

Fig 4 shows the enlarged portion of Fig 3 near the cooling channel where the prism layers are deployed.

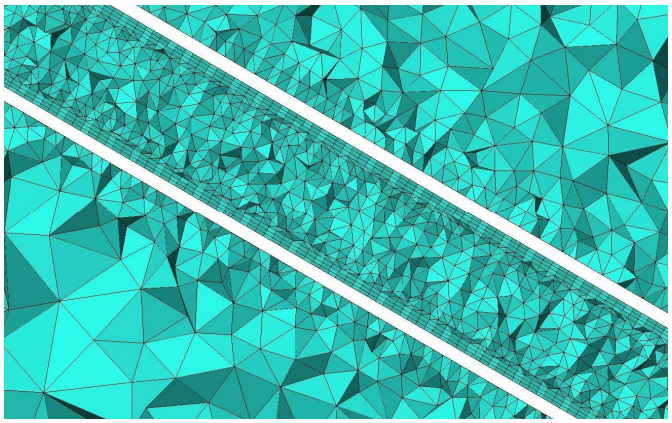

Figure 4: Mesh outline in the cooling channel of the combustor. Three layers of the prism type cells are generated near the walls.

Both Reynolds Averaged Navier-Stokes (RANS) and Large Eddy Simulation (LES) approaches are employed in this study. Due to strong anisotropic character of highly swirling flows, LES technique has been shown to be superior to RANS in accurately predicting turbulent mixing and combustion dynamics in highly swirling flows [5,6]. SST k-ω turbulence model [7,8] is used in Ansys CFX 12.1 to do the RANS computations. Smagorinski sub-grid scale model [9] together with Van-Driest near wall damping function is employed in OpenFOAM to perform the LES calculations. Due to the transient behaviour of the flow, unsteady form of the Navier-Stokes equations is solved in both cases. To advance the simulations to a fully developed state, steady state solution is used as the initial boundary condition in both RANS and LES computations. Several monitoring points are monitored in the model to make sure that the flow is fully developed. Thereafter, the sampling process is started and the time averaged parameters are calculated. Fig 5 and Fig 6 show the velocity fluctuations at three different monitor points and inlet average pressure fluctuations, respectively. The time step for the computations is 0.1 ms and sampling is started from the 1000th time step.

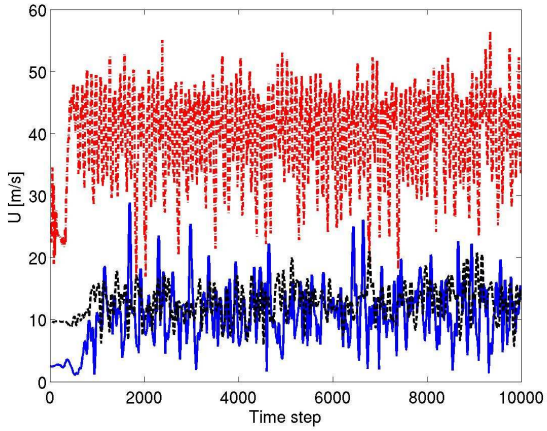

Figure 5 Velocity fluctuations at three different monitor points.

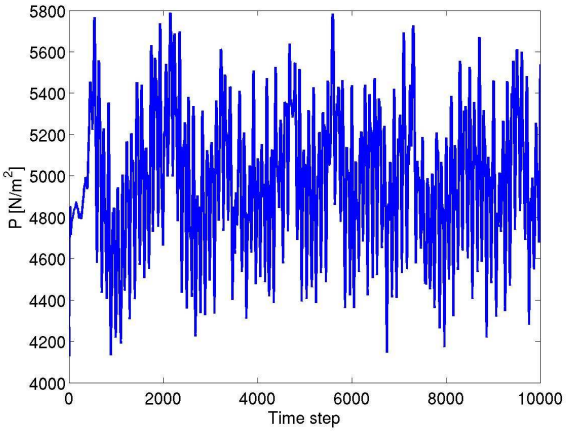

Figure 6: Average pressure fluctuations at the inlet of the diffuser.

RESULTS

Because of the size of the model, it is difficult to resolve the boundary layers unless a huge number of computational cells are deployed. To keep the mesh size reasonable, computational cells are mostly concentrated in the cooling channel and the center-line of the combustor. The flow which passes through the cooling channel ends up in the burner. Due to asymmetries that exist in the geometry of the combustor, it is important to study the air distribution in the cooling channel. A highly non-uniform flow in the cooling channel might impair the operation of the burner.

This study has focused on the diffuser, cooling channel, swirl generator and recirculation zone that are addressed in the following.

Diffuser

The distributions of the total and static pressures in the diffuser are shown in Fig 7.

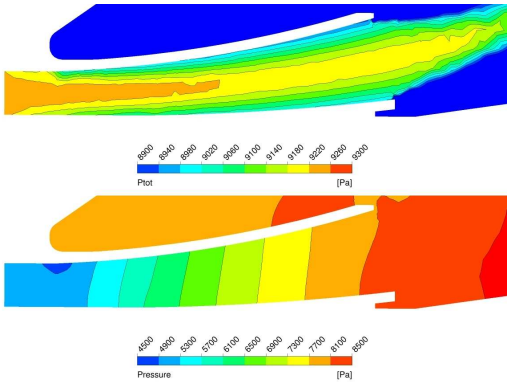

Figure 7: Total pressure (up) and static pressure (down) distribution in the diffuser.

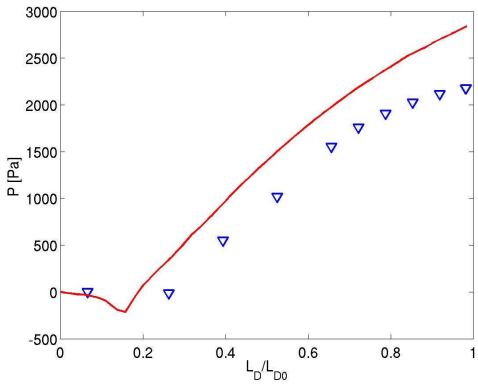

Figure 8: Static pressure along the upper wall of the diffuser. Line: CFD results; markers: measurements.

The comparison between the measured and computed static pressure along the upper wall of the diffuser is shown in Fig 8. It can be seen that the difference between the measurements and computations grow along the diffuser. One reason for this discrepancy might be the disturbances at the inlet of the diffuser in the experimental case. In case of CFD, the disturbances due to the turbulence are set to 5% of the mean flow which might be much less than that of the experiment. Besides, a constant velocity profile is applied at the inlet and the mesh is rather coarse in this region.

The static pressure distribution at the exit of the diffuser is shown in Fig 9. The effect of the struts on the pressure distribution can be seen clearly.

According to [10], the pressure recovery coefficient is defined as:

$$C_p = \frac{P_{st2} - P_{st1}}{P_{dyn}}$$

The computed C_p from the CFD and measured results is about 74% and 51%, respectively. The overall effectiveness is defined as:

$$\eta = C_p / C_{p-ideal}$$

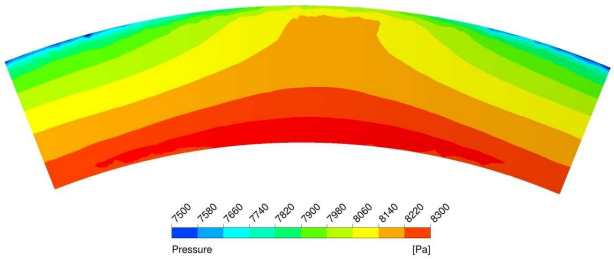

Figure 9: Static pressure distribution at the exit of the diffuser.

in which $C_{p\text{-ideal}}$ is defined as:

$$C_{p-ideal} = 1 - \frac{1}{AR^2}$$

Considering this definition, the overall effectiveness of diffuser based on the CFD calculations and measurements is 95% and 66%, respectively. This again suggests that the boundary conditions in CFD calculations are too ideal for the diffuser.

Cooling channel

Figs. 10 and 11 show the contours of the y^+ at the walls of the cooling channel. Only half of the cooling channel (180° sector) is shown in the pictures.

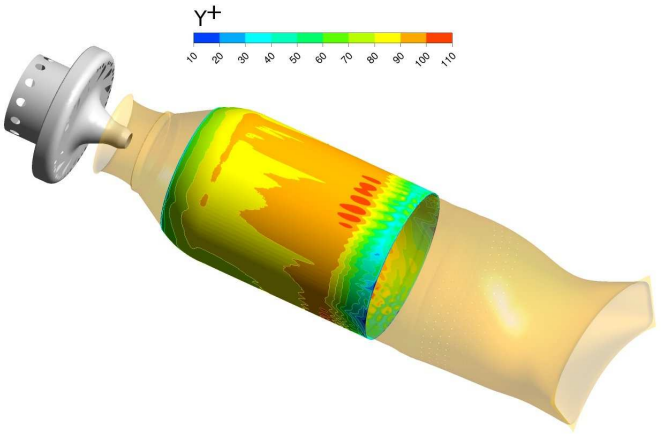

Figure 10: Distribution of y^+ along the inner wall of the cooling channel.

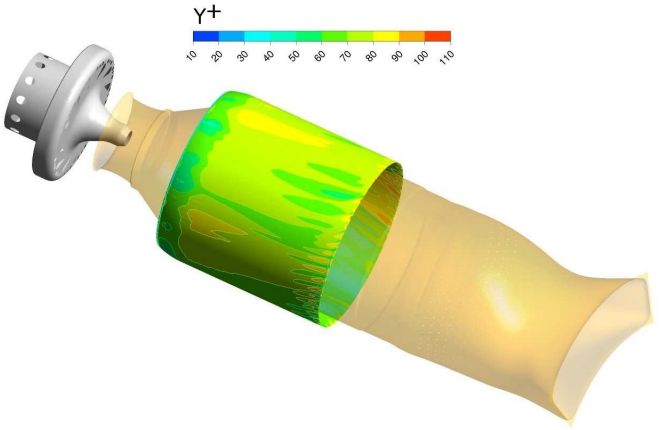

Figure 11: Distribution of the y^+ along the outer wall of the cooling channel.

The y^+ magnitudes on the inner wall of the cooling channel are slightly larger than those of the outer wall. Nevertheless, the values of y^+ in most part of the domain (in the cooling channel) are smaller than 100. Therefore the law of the wall (logarithmic distribution of the velocity near the wall) holds and wall functions can be applied appropriately.

In the experimental setup, the air mass flow rate is set to 1.8 kg/s from which the amount of the air that has passed through the main sector of the combustor is calculated to be 1 kg/s. This mass flux is applied as the boundary condition in CFD calculations.

Fig 12 compares the velocity distribution in the cooling channel at three different cross sections for the RANS and LES computations. The flow direction in the cooling channel is from right to left towards the pilot. It can be seen that the velocity of the air is higher in the upper part of the channel compared to the lower part in both pictures. The non-uniformity of the mass flux is at highest when the air enters the channel (the cross section which is marked by 0°, 90°, 180° and 270° angles).

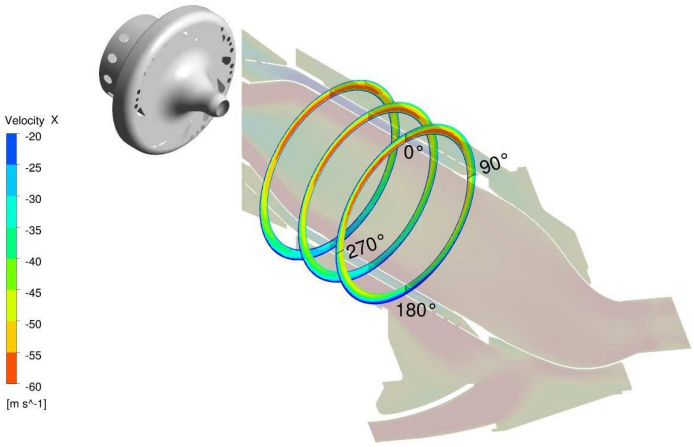

a) RANS.

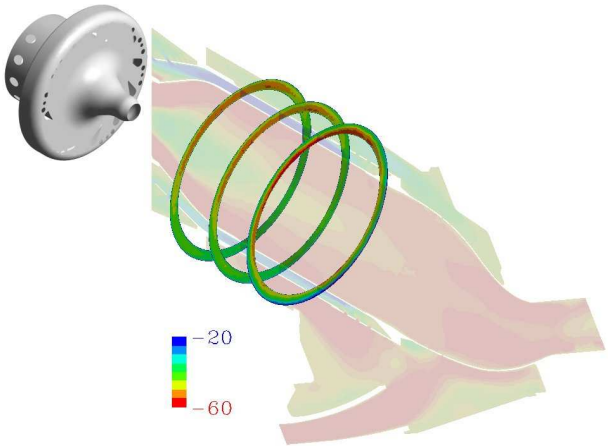

b) LES.

Figure 12: Comparison of the velocity distribution at three different cross sections in the cooling channel. The farthest cross section from the pilot is at the channel entrance and the closest cross section is at the exit of the channel. Angle is measured from the top of the channel (zero angle) in the clockwise direction.

Figs 13(a) and 13(b) show the comparison between measured and computed velocity profiles at the first and third cross sections at four angular positions (0°, 90°, 180° and 270°) that are shown in Fig 12.

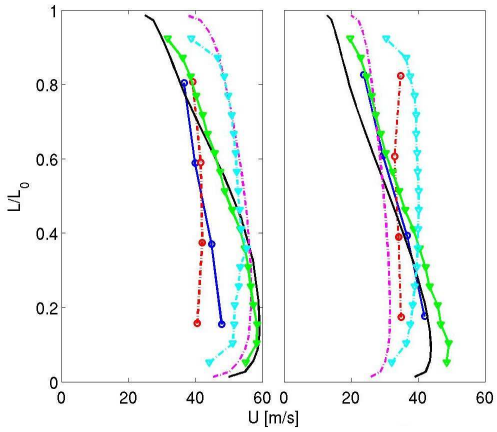

a) Velocity profiles at zero (left) and 180° (right).

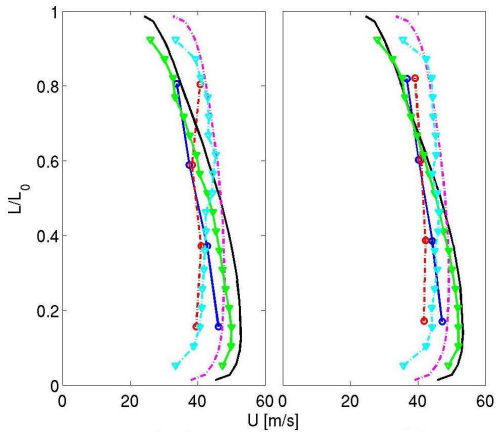

b) Velocity profiles at 90° (left) and 270° (right).

Figure 13: Velocity comparison at two cross sections in the cooling channel. Lines only: CFD-RANS; lines with triangle markers: CFD-LES; lines with circle markers: experiment. Continuous lines: entrance of the cooling channel; dashed lines: exit of the cooling channel.

The discrepancy between the measured and computed velocities is high. Nevertheless both experiment and computations confirm that the velocity magnitudes at 180° position are smaller than the rest of the channel. Besides, both simulations and experimental results confirm that the velocity profiles are more uniform at the exit of the channel compared to the inlet of the channel. However, the LES results show a more uniform distribution compared to RANS simulations.

Owing to the perfect symmetry of the CFD model which is due to the implementation of the periodic boundary condition in the angular direction, good agreement between the velocity profiles at 90° and 270° positions can be seen. In the experimental rig however, the slight differences between the pseudo-combustors and other geometry imperfections might have caused the differences in velocity profiles.

Recirculation zone and swirl generator

The contours of the axial velocity in the cooling channel and can are shown in Fig 14. In this figure, the extent of the recirculation zone where the axial velocity is zero is shown by the zero-velocity contour for both RANS and LES simulations. It is clear from the pictures that there exists a main recirculation zone in the can.

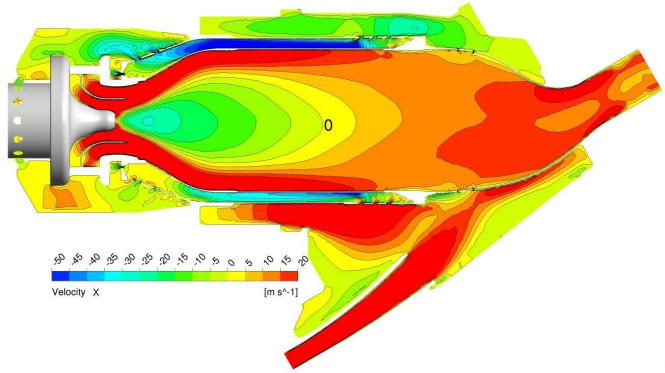

a) RANS.

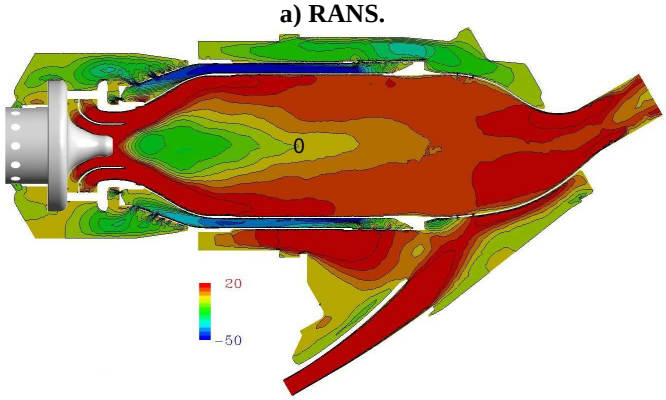

b) LES.

Figure 14: Comparison of contours of axial velocity in the can. The recirculation zone is marked by zero value.

LES predicts a smaller recirculation zone compared to RANS. This can be seen more clearly in Fig 15 which shows the predicted axial velocity along the center-line of the can in both simulations. It can be seen that the location of the backward stagnation point in both simulations coincides very well. However, this is not the case for the forward stagnation point. In case of the LES simulation, the forward stagnation points lies somewhat farther from the pilot exit.

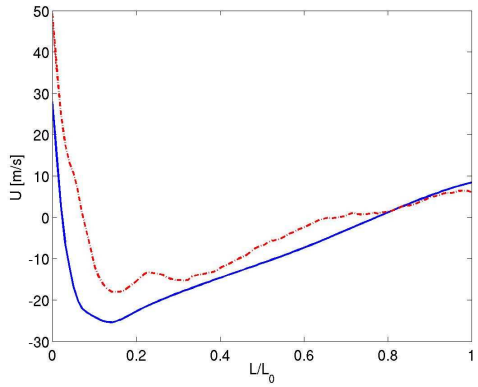

Figure 15: Axial velocity along the center-line of the can. Solid blue line: RANS model; dashed red line: LES simulation.

In the laboratory however, it was difficult to measure the recirculation extent in the can due to the complications in reaching the axis of the can by the designed pressure probe. Therefore, the experiment is done on a simplified model in which the diffuser and cooling channel are removed and a more simplified burner is installed. Unfortunately, the measurements on the simplified model show completely different result in comparison to the computations on the full scale model. The measured recirculation zone is much smaller than the computed one in the full-scale model. The ratio between the RANS computed and measured recirculation zone is about 4. Therefore the authors decided to run a case with simplified domain (similar to the experimental model) to study the effect of the simplification on the flow inside the can. All the boundary conditions are kept the same as the full model. The differences between the models are at the inlet where the flow enters the simplified model uniformly and at the pilot which is removed from the simplified case. The axial velocity contours of the simple model are shown in Fig 16.

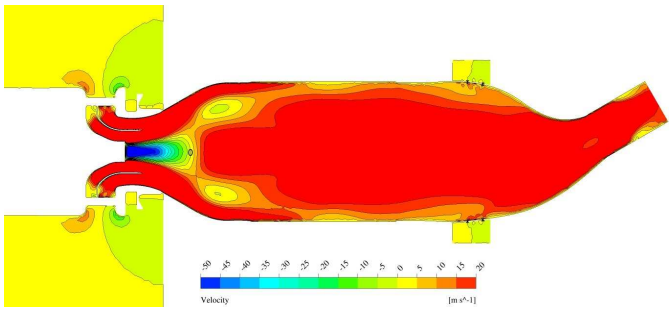

Figure 16: Contours of axial velocity in the simplified model.

The fluid flow behavior in the simplified model has completely changed with respect to the full model. Three small recirculation zones can be identified in the simplified model. The ratio between the computed and measured recirculation lengths is 1.07 which shows a good agreement.

In order to study the difference in behaviour of the flow, the cumulative swirl number is calculated along three sections that are shown in Fig. 17 (L1 near the exit of the swirl generator; L2 the smallest cross section of the burner and L3 in the middle of the recirculation zone).

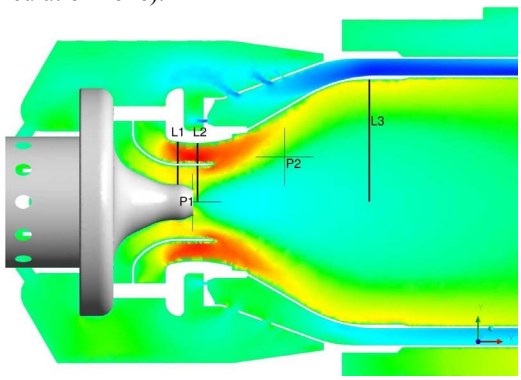

Figure 17: Three sections at which the cumulative swirl number is studied in different models (see Fig. 18). The locations at which the pressure is monitored are also shown.

Fig. 18 compares the variation of the cumulative swirl numbers at L1, L2 and L3 in simplified and full cases. The discontinuities in Fig 18(a) are due to the air splitter plate.

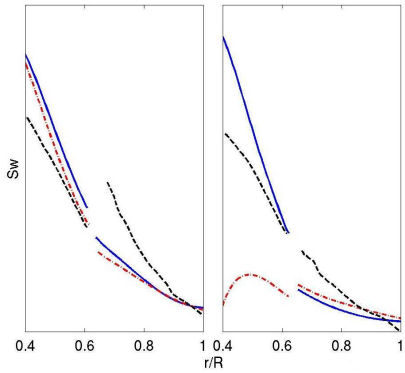

a) Swirl number at L1 (left) and L2 (right).

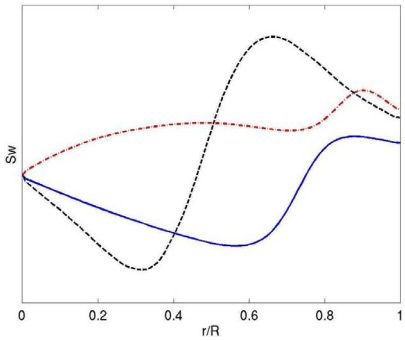

b) Swirl number at L3.

Figure 18: Variation of cumulative swirl number at different locations. Solid blue lines: full model RANS; dashed black lines: full model LES; dash-dotted red lines: simplified model RANS.

Due to confidentiality restrictions, the swirl axis values are dropped. Large differences can be observed between the results. At L1, good agreement between the total swirl numbers (the value of the Sw at the end of the lines) calculated by RANS and LES can be observed. Also the swirl numbers that are calculated by RANS show the same behaviour in both simplified and full models. LES however, yields higher tangential momentum at $r/R \approx 0.6$ in the outer channel.

At L2, both RANS and LES yield similar total swirl numbers in the inner channel for the full case. In the simplified case, the total swirl number is smaller than the full case. The behaviour of the swirl number is rather different between the cases. At the outer channel, RANS yields similar swirl numbers for both simplified and full cases which is somewhat higher than what LES calculation yields. In this part of the channel, the behaviour of the swirl number that is calculated by RANS is very similar between the simplified and full models whereas LES once again suggests higher tangential momentum near the wall.

At L3, no similar behaviour can be observed between the models. Since this location is out of the recirculation zone in simplified case, the swirl number is always positive due to a positive axial momentum. The difference between the LES and RANS results, suggests that the intensity of the recirculation zone is different between the cases.

The reason for this dramatic difference between the flows in the two models seems to be the existence of the pilot of the burner in the full scale model which is absent in the simplified model. The pilot creates a swirling flow that affects the main swirl. The computed results suggest that the influence of the swirling flow of the pilot is substantial on the formation of the recirculation region in the can.

Precessing vortex core

Precessing motions have been the subject of many studies in gas turbines. It is reported that the precessing motion improves the combustion efficiency [11] and the recirculation zone that exist in highly swirling flows plays an important role by providing a hot flow of recirculated combustion products. On the other hand, the unsteady motion caused by a precessing vortex can cause some damages by creating thermo-acoustic oscillations [12].

The characteristics of the swirling flows are studied in detail and are reviewed in several references (see [13-16]). It is observed that low frequency flow oscillations significantly affect the global behaviour of the flame [17]. In order to capture the dominant frequencies of the precessing vortex in SGT-750, the pressure is monitored in two points near the exit of the pilot and downstream of the burner at the border of the recirculation zone (see P1 and P2 in Fig 17), respectively. Figs. 19 and 20 show the transformed pressure fluctuations into frequency domain by help of the Fourier transform.

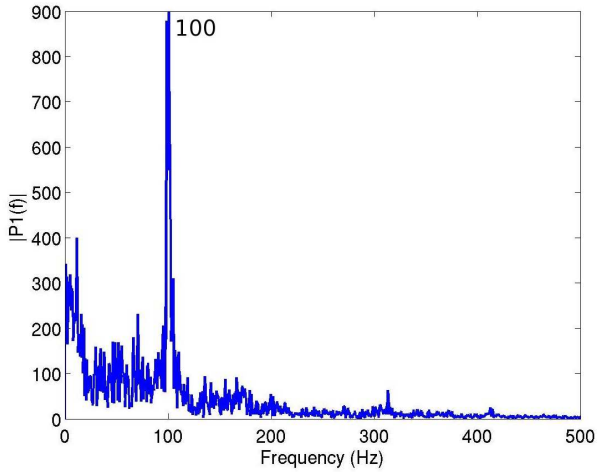

Figure 19: Fourier transformed pressure fluctuations at P1 (see Fig. 17).

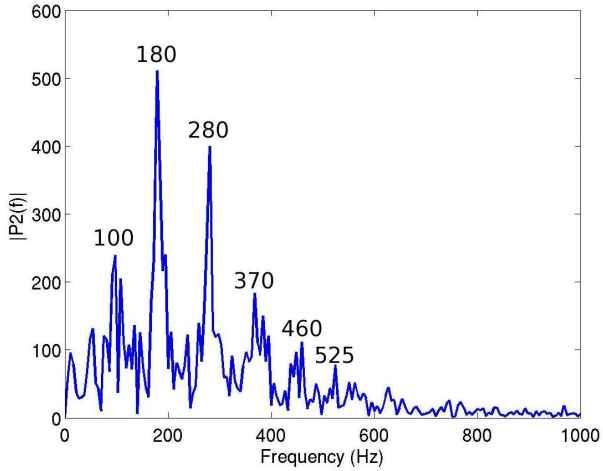

Figure 20: Fourier transformed pressure fluctuations at P2.

Fig. 19 shows a dominant 100 Hz signal at the exit of the pilot which is the rotational frequency of the precessing vortex core. At P2 several different frequencies are identifiable. The two most dominant frequencies, i.e. 180 and 280 Hz, might be related to the vortices that shed from the edge of the air splitter.

The precessing vortex core (PVC) is depicted in Fig. 21 by showing the iso-surfaces of the second invariant of the velocity field. The fact that the PVC is helical and wraps itself around the boundary of the recirculating flow zone [18] can be verified.

The contours of the temporal axial and tangential velocities in the can near the exit of the burner are shown in Figs 22 and 23, respectively. Matching regions of high axial and tangential velocities in red colour are identifiable in these pictures. The blue region in Fig. 22 depicts the reverse flow zone which is displaced from the central axis, however, the negative tangential velocities depicts the precessing vortex. The squeezing effect of this off-center reverse flow zone creates higher axial and tangential velocities near the wall.

The behaviour of the precessing vortex in this combustor is very similar to the described behaviour of the precessing vortex in reference [19]. Hence, whether or not the non-uniform distribution of the air in the cooling channel has affected the precessing vortex at the exit of the burner could not be identified.

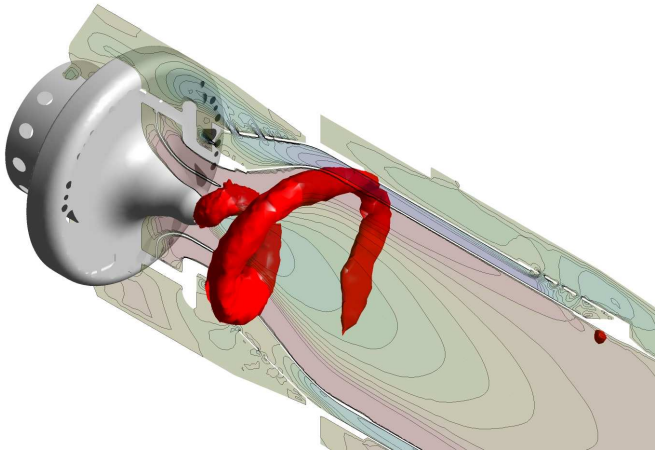

Figure 21: Precessing vortex core in the can.

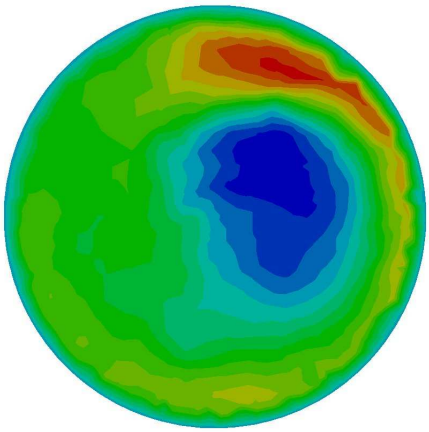

Figure 22: Axial velocity contours at the exit of the burner.

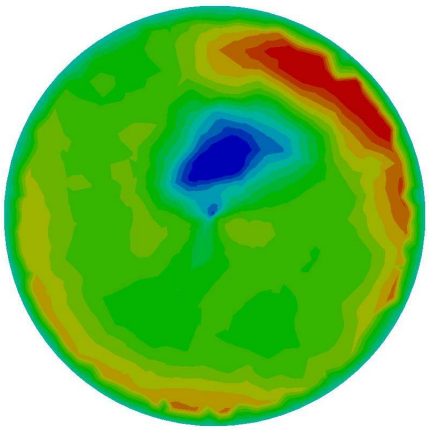

Figure 23: Tangential velocity contours at the exit of the burner.

CONCLUSIONS

Fluid flow is studied both experimentally and numerically in a combustor which is under development at Siemens Industrial Turbomachinery AB. The focus of this study is the cooling channel and recirculation zone in the can of the combustor. Two different computational methods, namely RANS and LES are used to study this combustor numerically. The computed velocity profiles at different cross sections of the cooling channel are compared to the measured ones and large discrepancies are observed although LES shows more promising results. Nevertheless, the results show the same trend and suggest that the air distribution is more uniform near the exit of the cooling channel.

Since it is difficult to measure the pressure along the centerline of the can in case of the full scale combustor, a simpler model is used for this purpose. It is shown by CFD that the flow behavior is completely different in case of the simple model. Large difference in the aerodynamic behavior of the flow seems to stem from the swirling flow of the pilot which is absent in case of the simple model.

CFD results show a more efficient diffuser compared to the measurements. It is believed that the low inlet turbulence intensity, the coarse mesh in case of CFD and effect of the walls in the experimental case have been the reasons why such a difference between the measured and computed results exists.

The precessing vortex core at the exit of the burner is studied and the dominant frequencies are computed from the pressure fluctuations. Regions of high axial and tangential velocities together with the vortex core are identified but no effect that could be related to the non-uniform distribution of the air in the cooling channel has been observed.

ACKNOWLEDGMENTS

The authors would like to acknowledge Siemens Industrial Turbomachinery AB, Finspong, Sweden for the permission to publish this paper. Additionally the authors acknowledge all Siemens employees involved in the development work during the concept, design and verification phases of the project. This work was financed by SIT.

REFERENCES

[1] Siemens gas turbines information available on: http://www.energy.siemens.com/hq/en/power-generation/gas-turbines/
[2] Siemens SGT-750 gas turbine. Information available on : http://www.energy.siemens.com/hq/en/power-generation/gas-turbines/sgt-750.htm
[3] Siemens SGT-500 gas turbine. Information available on: http://www.energy.siemens.com/hq/en/power-generation/gas-turbines/sgt-500.htm

[4] Schneider, C., Dreizler, A., Janicka, J., 2005, “Fluid Dynamical Analysis of Atmospheric Reacting and Isothermal Swirling Flows,” Flow, Turbulence and Combustion **74** pp. 103-127.
[5] Pierce, C., Moin, P., 1998, “Method for generating equilibrium swirling inflow conditions,” AIAA J. **36** pp. 1325–1327.
[6] Measurement of gas flow by means of critical flow Venturi nozzle, ISO9300.
[7] ANSYS CFD-Solver Theory Guide, Realease 12.1, November 2009.
[8] Wilcox, D.C., 2000, “Turbulence Modelling for CFD,” DCW Industries, La Canada, CA 91011.
[9] Smagorinsky, J., 1963, “General circulation experiments with the primitive equations,” Monthly Weather Review **91** pp. 99-165.
[10] Lefebvre, A. H., 2010, “Gas Turbine Combustion”, CRC Press.
[11] Wong, C. Y., Nathan, G. J., O’Doherty, T., 2004, “The effect of initial conditions on the exit flow from a fluidic precessing jet nozzle,” Exp. Fluids **36** pp. 70–81.
[12] Syred, N., Beer, J. M., 1974, “Combustion in swirling flows: a review,” Combustion and Flame **23** pp. 143-201.
[13] Lilley, D. G., 1977, “Swirl flows in combustion: A review,” AIAA J. **15** pp 1063-1078.
[14] Coats, C. M., 1996, “Coherent structures in combustion,” Prog Energy Combust. Sci. **22** pp. 427-509.
[15] Lucca-Negro, O., O’Doherty, T., 2001, “Vortex breakdown: a review,” Progress in Energy and Combustion Science **27** pp. 431-481.
[16] Syred, N., 2006, “A review of oscillation mechanisms and the role of the orecessing vortex core (PVC) in swirl combustion systems,” Progress in Energy and Combustion Science **32** pp. 93-161.
[17] Huang, Y., Yang, V., 2005, “Effect of swirl on combustion dynamics in a lean-premixed swirl-stabilized combustor,” Proceedings of the Combustion Institute **30** pp. 1775-1782.
[18] Chanaud, R. C., 1965, “Observations of oscillatory motion in certain swirling flows,” J. Fluid Mechanics **21** pp. 111.
[19] Froud, D., O’Doherty, T., Syred, N., “Phase averaging of the precessing vortex core in a swirl burner under piloted and premixed combustion conditions,” Combustion and Flame **100** pp. 407-412.